Interference Carpets in Above-Threshold Ionization: From the Coulomb-Free to the Coulomb-Dominated Regime

Ph. A. Korneev, S. V. Popruzhenko, and S. P. Goreslavski
National Research Nuclear University MEPhI, Kashirskoe Shosse 31, 115409, Moscow, Russia

T.-M. Yan
Institut für Physik, Universität Rostock, 18051 Rostock, Germany
and Max-Planck-Institut für Kernphysik, Postfach 103980, 69029 Heidelberg, Germany

D. Bauer
Institut für Physik, Universität Rostock, 18051 Rostock, Germany

W. Becker
Max-Born-Institut, Max-Born-Str. 2a, 12489 Berlin, Germany

M. Kübel and M. F. Kling
Max-Planck-Institut für Quantenoptik, 85748 Garching, Germany

C. Rödel, M. Wünsche, and G. G. Paulus
Institute of Optics and Quantum Electronics, Friedrich Schiller University, Max-Wien-Platz 1, 07743 Jena, Germany
(Received 9 March 2012; published 31 May 2012)

The velocity map recorded in above-threshold ionization of xenon at 800 nm exhibits a distinct carpetlike pattern of maxima and minima for emission in the direction approximately perpendicular to the laser polarization. The pattern is well reproduced by a numerical solution of the time-dependent Schrödinger equation. In terms of the simple-man model and the strong-field approximation, it is explained by the constructive and destructive interference of the contribution of the long and the short orbit. Strictly perpendicular emission is caused by ionization at the two peaks of the laser field per cycle, which results in a $2\hbar\omega$ separation of the above-threshold ionization rings.

DOI: 10.1103/PhysRevLett.108.223601 PACS numbers: 42.50.Hz, 32.80.Qk, 32.80.Rm, 34.50.Rk

An atom in the presence of a laser field strong enough to ionize emits a sequence of electronic wave packets [1]. An analysis in momentum space will record a richly structured interference pattern whose origin is the oscillatory behavior of the laser field and the ensuing modulation of the wave packet [2]. From an S-matrix point of view, there are several different pathways that lead from a specified electronic initial state, viz., the atomic ground state, into a specified final state, viz., the final momentum state, which is measured by the detector. The superposition of their contributions in the quantum-mechanical ionization amplitude causes the interference pattern. If the field is periodic with period T, superposition of the contributions from different cycles will generate sharp peaks in energy, which are separated by $\hbar\omega = h/T$ [3,4]. Since the same final momentum state can be reached via at least two different electron orbits within one cycle, there is an additional structure with an energy separation of more than $\hbar\omega$ superimposed on the former [3,4].

Previous attention has focused on emission in the direction of the laser-field polarization, where the spectrum is largely shaped by the classical motion in the laser field (plus the Coulomb field). It displays the effects for which above-threshold ionization (ATI) is known, e.g., the rescattering-related plateau and the steep drop of the spectral yield from low energies to the onset of the plateau; see, e.g., the review [5,6]. In this Letter, we focus on emission at almost right angle to the laser-field polarization. We report the observation of a very regular grid of sharply defined interference peaks in momentum space. However, in marked contrast to emission in the longitudinal direction, the energy spacing of the peaks strictly in the transverse direction is $2\hbar\omega$ corresponding to generation times that are only $T/2$ apart.

In our experiment, using a velocity map imaging spectrometer, we have measured angle-resolved photoelectron spectra of several rare-gas species ionized by a Ti:Sapphire laser (Femtolasers Compact Pro CEP). We used a pulse duration of 25 fs, the pulse energy was 1 mJ, and the wavelength 800 nm. Figure 1 shows a typical momentum spectrum in false-color representation. The color scale was adjusted such that quick color transitions due to the steep roll-off of counting rates toward increasing electron momentum do not obstruct the visibility of structures in the spectra. The spectrum is dominated by a series of concentric rings centered at zero momentum, which correspond

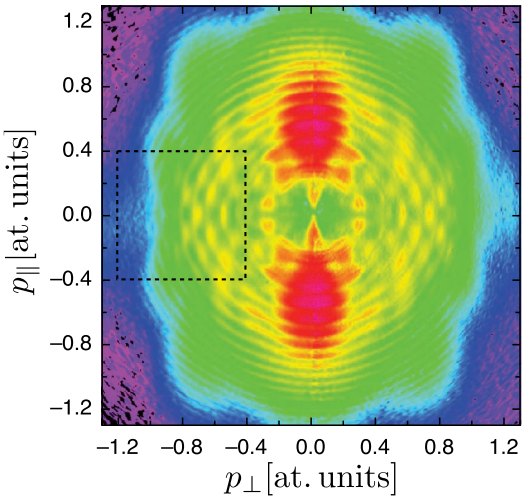

FIG. 1 (color online). Measured velocity map for ionization of xenon by a 25 fs 800 nm Ti:Sa laser pulse with an energy of 1 mJ. The laser polarization is in the vertical direction. The dashed-line bordered rectangle indicates the region depicted in Fig. 2.

to the characteristic ATI peaks. However, the yield along any such ring strongly depends on the direction of emission. In the direction of the polarization axis, all rings exhibit maxima, while exactly perpendicularly to it, every other ring has a minimum. In momentum space, the minima (and the maxima as well) lie on smooth curves, which together with the ATI rings define a very regular carpetlike pattern. It can be envisioned as a far-field continuum version of a "quantum carpet" [7].

The principal reason for the absence of every other peak for perpendicular emission can be explained remarkably simply: According to the simple-man model [8], electrons will have zero drift energy in the polarization direction if they are injected into the continuum at times when the laser field is extremal. In each cycle, there are two such extrema, with the field pointing in opposite directions. But the direction of the (longitudinal) field does not matter for perpendicular emission. Therefore, the electron emission events at the field's extrema, which are spaced by $T/2$, are indistinguishable, which results in a spectrum with lines separated by twice the photon energy, every other line being eliminated by destructive interference. An alternative explanation for this feature, for an infinitely long sinusoidal laser pulse, involves the dipole selection rules: as each final state corresponds to a certain net number of photons absorbed from the laser field, it can only contain either odd or even angular momenta. Clearly, for a final state which only contains odd angular momenta, the probability density is exactly zero in the plane perpendicular to the polarization direction. In other words, for sufficiently long pulses with well-defined photon energies, this feature is exact.

The absence of every other ATI peak for perpendicular emission is implicit already in the earliest papers [9], but the effect has received little attention. The first explicit discussion may be in Ref. [10]. In simulations based on numerical solutions of the time-dependent Schrödinger equation (TDSE) it is quite visible [11–13]. Experimentally, there is a (with hindsight) very distinct observation in Ref. [14]. Subsequent recordings were only recent [15,16]; however, these papers were focused on cluster behavior and different features of the ATI spectrum ("photoelectron holography" [17]), respectively.

The carpetlike pattern that develops for $p_\parallel \neq 0$ can be understood by a generalization of the argument presented above. For this we turn to the strong-field approximation (SFA) [9,18–21]. In the saddle-point approximation, the ionization amplitude $M_{\mathbf{p}}$ for specified $\mathbf{p} \equiv (p_\parallel, p_\perp)$ is the coherent sum of the contributions of "quantum orbits," which start at certain times $t_i \equiv t_{0i}(\mathbf{p})$ at the position where the electron tunnels to freedom, are subsequently governed by the laser field only with the Coulomb field neglected, and finally at the end of the laser pulse have acquired the momentum $\mathbf{p}$,

$$M_{\mathbf{p}} = \sum_i a_i(\mathbf{p}) \exp[-iS_i(\mathbf{p})]. \tag{1}$$

The actions are (we use atomic units such that $\hbar = m = |e| = 4\pi\epsilon_0 = 1$)

$$S_i(\mathbf{p}) = \frac{1}{2}\int_{t_i} d\tau[\mathbf{p} + \mathbf{A}(\tau)]^2 - I_p t_i, \tag{2}$$

and the complex ionization times t_i are determined as solutions of the saddle-point equation

$$\tfrac{1}{2}[p_\perp^2 + (p_\parallel + A(t_i))^2] = -I_p, \tag{3}$$

where $I_p > 0$ denotes the ionization potential. For the linearly polarized field

$$A(t) = A_0 \cos\omega t, \tag{4}$$

with the ponderomotive potential $U_p = A_0^2/4$, there are two solution times t_1 and t_2 ($\mathrm{Re}t_2 > \mathrm{Re}t_1$) per cycle, which satisfy

$$\mathrm{Re}\,\omega t_2 = 2\pi - \mathrm{Re}\omega t_1, \qquad \mathrm{Im}\omega t_1 = \mathrm{Im}\omega t_2 \tag{5}$$

(we are only concerned with the physical solutions in the upper half ωt plane, which are those through which the steepest-descent contour is routed).

In the length-gauge SFA, the weights of the two quantum orbits are

$$a_i(\mathbf{p}) = \left(\frac{2\pi}{i[\mathbf{p} + \mathbf{A}(t_i)] \cdot \mathbf{E}(t_i)}\right)^{1/2} \times \int d^3\mathbf{r} e^{-i[\mathbf{p}+\mathbf{A}(t_i)]\cdot\mathbf{r}} V(r)\psi_0(\mathbf{r}). \tag{6}$$

For the two saddle-point times t_i, the first factor is real and identical up to the small imaginary part of $\mathbf{E}(t_i)$, which we neglect. The second factors are equal for an even-parity

ground state $|\psi_0\rangle$ and equal in magnitude but opposite in sign for an odd-parity ground state (for $p_\parallel = 0$) [22].

We will be concerned with a p ground state and, therefore, assume that $a_1(\mathbf{p}) = -a_2(\mathbf{p})$. The two quantum orbits then will interfere destructively if [23]

$$\mathrm{Re}\,\Delta S \equiv \mathrm{Re}[S_2(\mathbf{p}) - S_1(\mathbf{p})] = 2n\pi. \tag{7}$$

Actually, due to the properties (5), it turns out that ΔS is automatically real. The condition (7) defines curves in $(p_\parallel, p_\perp)$ space along which $d\Delta S = 0$. With some algebra, we find that these curves (and, actually, any curve with $\Delta S = \mathrm{const}$) satisfy the first-order nonlinear differential equation

$$\frac{dE}{dp_\parallel} = -\frac{1}{t_2 - t_1}\int_{t_1}^{t_2} d\tau A(\tau), \tag{8}$$

where $E = (p_\parallel^2 + p_\perp^2)/2$ and the right-hand side depends on $p_\parallel$ and $p_\perp$ via t_2 and t_1. The right-hand side of the differential Eq. (8) is positive, and one can convince oneself that qualitatively it generates the behavior observed in the numerical simulations and the experimental data.

For the field (4), the saddle-point Eq. (3) has the solution

$$\cos^2(\mathrm{Re}\,\omega t_2) = \frac{\alpha}{2} - \frac{1}{2}\sqrt{\alpha^2 - \frac{p_\parallel^2}{U_p}}, \tag{9a}$$

$$\cosh(\mathrm{Im}\,\omega t_2) = -\frac{p_\parallel}{2\sqrt{U_p}\cos(\mathrm{Re}\,\omega t_2)}, \tag{9b}$$

where $\gamma^2 = I_p/(2U_p)$ denotes the Keldysh parameter and

$$\alpha = 1 + \gamma^2 + \frac{p_\parallel^2 + p_\perp^2}{4U_p}. \tag{10}$$

In the limit where $p_\parallel \to 0$, we have $\cosh(\mathrm{Im}\,\omega t_2) \to \sqrt{\alpha(p_\parallel = 0)}$. The other solution t_1 is specified by Eq. (5). Taking into account Eqs. (9), one obtains for the phase difference

$$\Delta S = \left[\frac{1}{2}(p_\perp^2 + p_\parallel^2) + I_p + U_p\right](t_2 - t_1) - \frac{p_\parallel^2}{\omega} \times \tan(\omega\,\mathrm{Re}\,t_2) - \frac{2U_p}{\omega}\sin(\omega\,\mathrm{Re}\,t_2)\cos(\omega\,\mathrm{Re}\,t_2). \tag{11}$$

For purely perpendicular emission, so that $p_\parallel = 0$, we have from Eq. (9a) that $\omega(t_2 - t_1) = \pi$, $\cos(\omega\,\mathrm{Re}\,t_2) = 0$. The destructive-interference condition (7) then reduces to

$$\Delta S = \left(\frac{1}{2}p_\perp^2 + I_p + U_p\right)(t_2 - t_1) = 2n\pi. \tag{12}$$

On the Nth ATI ring, we have $p_\perp^2/2 + I_p + U_p = N\omega$ so that the condition reads

$$N = 2n. \tag{13}$$

This confirms that for emission at right angle to the laser polarization direction, ATI rings with even order N are absent due to destructive interference of the two contributing quantum orbits.

Figure 2 compares the velocity maps of the experimental data [panel (a), which is a blow-up of Fig. 1], of a solution of the three-dimensional TDSE [panel (b)], and of the SFA calculation [panel (c)]. The data exhibit a very distinct carpetlike rhombic pattern, which is best developed in the region of the ATI rings $N = 13, \ldots, 16$. The TDSE was solved for a trapezoidal pulse with a flat part of

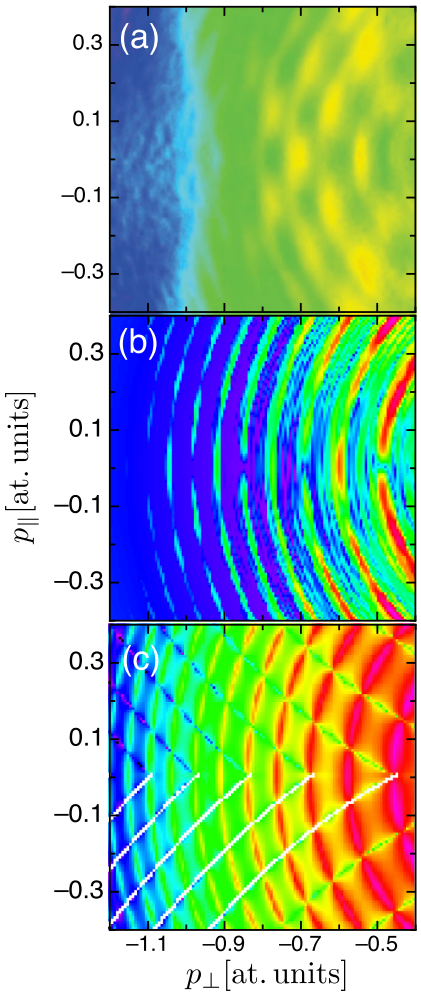

FIG. 2 (color online). The carpet region: (a) blow-up of the experimental data of Fig. 1; (b) TDSE simulation for a (2, 5, 2) pulse with peak field $\omega A_0 = 0.0427$ a.u. ($I = 6.43 \times 10^{13}$ W/cm^2, $U_p = 3.73$ eV $= 0.137$ a.u.), frequency $\omega = 0.05768$ a.u. (1.57 eV, 789.9 nm), and ionization potential $I_p = 0.44435$ a.u. $= 12.06$ eV; (c) SFA simulation, evaluated for the same pulse as used for the TDSE. The SFA was calculated via the saddle-point approximation for a monochromatic field and the δ functions of the ATI peaks were broadened by hand to account for the finite pulse duration. The white lines in panel (c) represent the solutions of Eq. (8). The lowest-energy ATI ring having a maximum at $p_\parallel = 0$ is $N = 13$ at approximately $p_\perp = 0.6$ a.u.

5 cycles and 2 cycles turn-on and turn-off. It predicts, as expected, the sequence of interference maxima and minima on the $p_\perp$ axis on subsequent ATI rings. The carpetlike rhombic pattern is very pronounced, too, but only for the higher ATI rings as of $N = 16$. This is a rare example of a pronounced qualitative effect that is more clearly developed in the data than in a TDSE simulation. The SFA also yields a very regular pattern, as predicted by the analytical results above. However, as discussed below, it appears squeezed toward smaller values of $|p_\parallel|$. The destructive-interference curves, which are the solutions of Eq. (8), practically agree with the conical lines in Fig. 2(c) that emanate from the $p_\perp$ axis.

The discrepancies between the experimental data and the SFA reveal the long-range effect of the Coulomb potential, which is not accounted for by the SFA. This can be quantified, for example, along the ATI ring $N=15$ (which has a maximum on the $p_\perp$ axis) within the angular range covered by the figure one counts 5 interference maxima in the data, while the SFA yields 7. For the higher-order rings, comparison of the SFA and the TDSE exhibits an increasing discrepancy (e.g., for $N = 20$, it is 4 maxima for the TDSE vs 8 for the SFA).

With account of the Coulomb potential, the matrix element can still be decomposed into the contribution of quantum orbits in the fashion of Eq. (1). However, the orbits and their actions (2) must be modified to include the effect of the Coulomb potential [24,25]. The fact that the $\Delta S = \text{const}$ curves are steeper in reality than in the SFA indicates that along an ATI ring the Coulomb potential slows down the variation of ΔS. This is reflected both in the slope of the curves when they depart from the $p_\perp$ axis and in the number of interference minima on a given ATI ring.

In an attempt qualitatively to understand this behavior, we notice that the dominant effect of the Coulomb potential is to replace ΔS by $\mathcal{V}_2 - \mathcal{V}_1 + \mathcal{T}_2 - \mathcal{T}_1 - I_p(t_2 - t_1)$, where $\mathcal{V}_i = -\int_{t_i}^{\infty} d\tau/|\mathbf{r}_i(\tau)|$ and $\mathcal{T}_i = \int_{t_i}^{\infty} d\tau \mathbf{v}^2/2$ are the integrals along the outgoing orbit $i = 1$ or $i = 2$ [24]. The two integrals $\mathcal{V}_1$ and $\mathcal{V}_2$ are exactly equal for perpendicular emission. In contrast, for parallel emission they are maximally different: having exited the tunnel, both orbits initially are accelerated away from the ion. When the field changes sign, the earlier orbit (the long orbit $i = 1$) turns around and then traverses the Coulomb potential, having a nonvanishing initial transverse momentum, which asymptotically will be compensated by the Coulomb force. On the other hand, the later orbit (the short orbit $i = 2$) continues to follow its original direction away from the ion. Therefore, $|\mathcal{V}_1| > |\mathcal{V}_2|$ for $p_\perp \neq 0$. Since ΔS is positive, the net effect of the Coulomb potential is to increase ΔS, especially so in predominantly parallel emission. However, the Coulomb field also enters the kinetic-energy term of the action, $\mathcal{T}_2 - \mathcal{T}_1$. On the long orbit, the electron has a higher kinetic energy while it is near its parent ion because it is temporarily accelerated by the Coulomb potential and because of the extra initial transverse momentum. This gives another Coulomb-caused contribution to ΔS, which is negative. In the situation of this Letter, the latter is dominant. Hence, the effect of the Coulomb contributions is subtle but, on the other hand, it allows detailed insight into the laser-controlled electron dynamics. The matter is further complicated by the fact that, for given final momentum, the Coulomb potential also modifies the initial times t_i and that qualitatively new orbits exist; see below.

Inspection of Fig. 2(c) shows that the pertinent part of the SFA velocity map is dominated by two sets of curves: the (concentric) ATI rings and, on the other hand, the curves $\Delta S = 2n\pi$ that connect the interference minima and intersect the ATI rings [26]. It was recently found [17,25] that the Coulomb field introduces new types of trajectories, which do not exist in the SFA. These new trajectories make an important contribution inside a cone along the polarization direction, while for small longitudinal and relatively large lateral momenta still just the two standard SFA trajectories (ionization times t_1 and t_2) contribute, although they are distorted by the Coulomb field. Therefore, the SFA pattern of Fig. 2(c) describes the data qualitatively for large emission angles, though the Coulomb field quantitatively modifies the actions (2) as discussed above. In contrast, emission closer to the polarization direction is essentially affected by the Coulomb field so that there is not even qualitative agreement [24,25]. Hence, we have established the existence of two parts of the photoelectron momentum distribution, one strongly affected by the Coulomb interaction and the other one only moderately. The latter remains the natural object for applying the SFA.

In summary, we reported the observation of a very regular carpetlike pattern in the velocity map of atomic ATI, which dominates the spectrum at emission sufficiently far away from the field-polarization axis. Good agreement was demonstrated with solutions of the TDSE. We also simulated the spectrum within the SFA taking into account the two direct intracycle electron orbits (rescattering was not considered) that lead into a final state with given momentum. The constructive and destructive interference of these two orbits, and the ATI rings, which are generated by constructive interference of the orbits of *all* laser cycles [3,4], determine the gross structure of the angle-resolved spectrum. The resulting pattern is distorted by the Coulomb potential but qualitatively preserved at sufficiently large angles of emission with respect to the laser polarization. Quantitative measures of the distortion were discussed. With the help of these tools, it may be possible to analyze and quantify the consequences of the Coulomb-bound electron dynamics for atoms and molecules.

We are grateful to D. B. Milošević, W. P. Schleich, and O. Smirnova for illuminating discussions. This work was

supported in part by the Russian Foundation of Basic Research (Project No. 11-02-91331) and the Deutsche Forschungsgemeinschaft (Kl-1439/2, Pa-730/4, Sm-292/1, and SFB 652). T. M. Y. acknowledges support from the International Max Planck Research School for Quantum Dynamics in Heidelberg.

[1] H. G. Muller and F. C. Kooiman, Phys. Rev. Lett. **81**, 1207 (1998).
[2] R. Gopal, K. Simeonidis, R. Moshammer, Th. Ergler, M. Dürr, M. Kurka, K.-U. Kühnel, S. Tschuch, C.-D. Schröter, D. Bauer, J. Ullrich, A. Rudenko, O. Herrwerth, Th. Uphues, M. Schultze, E. Goulielmakis, M. Uiberacker, M. Lezius, and M. F. Kling, Phys. Rev. Lett. **103**, 053001 (2009).
[3] D. B. Milošević, G. G. Paulus, and W. Becker, Phys. Rev. A **71**, 061404(R) (2005).
[4] D. G. Arbó, K. L. Ishikawa, K. Schiessl, E. Persson, and J. Burgdörfer, Phys. Rev. A **81**, 021403(R) (2010).
[5] W. Becker, F. Grasbon, R. Kopold, D. B. Milošević, G. G. Paulus, and H. Walther, Adv. At. Mol. Opt. Phys. **48**, 35 (2002).
[6] D. B. Milošević, G. G. Paulus, D. Bauer, and W. Becker, J. Phys. B **39**, R203 (2006).
[7] A. E. Kaplan, I. Marzoli, W. E. Lamb, Jr., and W. P. Schleich, Phys. Rev. A **61**, 032101 (2000).
[8] H. B. van Linden van den Heuvell and H. G. Muller, in *Multiphoton Processes* edited by S. J. Smith and P. L. Knight (Cambridge University Press, Cambridge, 1988), Vol. 8, p. 25.
[9] A. M. Perelomov, V. S. Popov, and M. V. Terent'ev, Zh. Eksp. Teor. Fiz. **50**, 1393 (1966) [Sov. Phys. JETP **23**, 924 (1966)].
[10] G. F. Gribakin and M. Yu. Kuchiev, Phys. Rev. A **55**, 3760 (1997).
[11] E. A. Volkova, A. M. Popov, and O. V. Tikhonova, Zh. Eksp. Teor. Fiz. **120**, 1336 (2001) [JETP **93**, 1155 (2001)].
[12] Z. Chen, T. Morishita, A.-T. Le, M. Wickenhauser, X. M. Tong, and C. D. Lin, Phys. Rev. A **74**, 053405 (2006).
[13] X.-B. Bian, Y. Huismans, O. Smirnova, K.-J. Yuan, M. J. J. Vrakking, and A. D. Bandrauk, Phys. Rev. A **84**, 043420 (2011).
[14] M. J. Nandor, M. A. Walker, and L. D. Van Woerkom, J. Phys. B **31**, 4617 (1998).
[15] S. Zherebtsov, Th. Fennel, J. Plenge, E. Antonsson, I. Znakovskaya, A. Wirth, O. Herrwerth, F. Süßmann, C. Peltz, I. Ahmad, S. A. Trushin, V. Pervak, S. Karsch, M. J. J. Vrakking, B. Langer, C. Graf, M. I. Stockmann, F. Krausz, E. Rühl, and M. F. Kling, Nature Phys. **7**, 656 (2011).
[16] T. Marchenko, Y. Huismans, K. J. Schafer, and M. J. J. Vrakking, Phys. Rev. A **84**, 053427 (2011).
[17] Y. Huismans, A. Rouzée, A. Gijsbertsen, J. H. Jungmann, A. S. Smolkowska, P. S. W. M. Logman, F. Lépine, C. Cauchy, S. Zamith, T. Marchenko, J. M. Bakker, G. Berden, B. Redlich, A. F. G. van der Meer, H. G. Muller, W. Vermin, K. J. Schafer, M. Spanner, M. Yu. Ivanov, O. Smirnova, D. Bauer, S. V. Popruzhenko, and M. J. J. Vrakking, Science **331**, 61 (2011).
[18] L. V. Keldysh, Zh. Eksp. Teor. Fiz. **47**, 1945 (1964) [Sov. Phys. JETP **20**, 1307 (1965)]; F. H. M. Faisal, J. Phys. B **6**, L89 (1973); H. R. Reiss, Phys. Rev. A **22**, 1786 (1980).
[19] G. G. Paulus, F. Zacher, H. Walther, A. Lohr, W. Becker, and M. Kleber, Phys. Rev. Lett. **80**, 484 (1998).
[20] S. P. Goreslavskii, S. V. Popruzhenko, N. I. Shvetsov-Shilovskii, and O. V. Shcherbachev, Zh. Eksp. Teor. Fiz. **127**, 27 (2005) [JETP **100**, 22 (2005)].
[21] T. Remetter, P. Johnsson, J. Mauritsson, K. Varjú, Y. Ni, F. Lépine, E. Gustafsson, M. Kling, J. Khan, R. López-Martens, K. J. Schafer, M. J. J. Vrakking, and A. L'Huillier, Nature Phys. **2**, 323 (2006).
[22] D. Bauer, D. B. Milošević, and W. Becker, Phys. Rev. A **72**, 023415 (2005).
[23] For an even-parity ground state, here and below, $2n$ has to be replaced by $2n + 1$.
[24] S. V. Popruzhenko and D. Bauer, J. Mod. Opt. **55**, 2573 (2008); S. V. Popruzhenko, G. G. Paulus, and D. Bauer, Phys. Rev. A **77**, 053409 (2008).
[25] T.-M. Yan, S. V. Popruzhenko, M. J. J. Vrakking, and D. Bauer, Phys. Rev. Lett. **105**, 253002 (2010).
[26] The SFA predicts another set of destructive-interference curves with $\Delta S = 2n\pi$. These curves do not intersect the $p_\perp$ axis at all. They are obtained as solutions of the differential Eq. (8) with the initial condition that $\Delta S = 2n\pi$ at values $p_{\parallel n}$ and $p_\perp = 0$. They are very dominant in the complete velocity maps of photodetachment of negative ions but not at all visible in Fig. 1. They will be discussed elsewhere. In the available experimental angle-resolved spectra for negative ions [A. Gazibegović-Busuladžić, D. B. Milošević, W. Becker, B. Bergues, H. Hultgren, and I. Yu. Kiyan, Phys. Rev. Lett. **104**, 103004 (2010)] one of those curves may be visible.